HHS Public Access

Author manuscript

Ultrasound Med Biol. Author manuscript; available in PMC 2019 March 01.

Published in final edited form as:

Ultrasound Med Biol. 2018 March ; 44(3): 622–634. doi:10.1016/j.ultrasmedbio.2017.11.005.

Investigation of optimized treatment conditions for acoustic-transfection technique for intracellular delivery of macromolecules

Min Gon Kim[1], **Sangpil Yoon**[1,*], **Chi Tat Chiu**[1], and **K. Kirk Shung**[1]

[1]Department of Biomedical Engineering, University of Southern California, Los Angeles, CA, 90089

Abstract

Manipulation of cellular functions and structures by introducing genetic materials inside cells has been one of the most prominent research areas in biomedicine. Acoustic-transfection with high frequency ultrasound has recently been developed and confirmed by intracellular delivery of small molecules into HeLa cell at single-cell level with high cell viability. After we proved the concept of acoustic-transfection technique, intensive investigation of treatment conditions between different human cancer cell lines has been performed to further develop acoustic-transfection as a versatile and adaptable transfection method by satisfying requirements of high delivery efficiency and cell membrane permeability with minimal membrane disruption. To determine optimal treatment conditions for different cell lines, we developed a quantitative intracellular delivery score (IDS) based on delivery efficiency, cell membrane permeability and cell viability after 4 and 20 hours of treatment. The intracellular delivery of macromolecule and simultaneous intracellular delivery of two molecules with optimal treatment conditions were successfully achieved. We demonstrated that DNA plasmid was delivered by acoustic-transfection technique into epiblast stem cells, which expressed transient mCherry fluorescence.

Keywords

Acoustic-transfection with high frequency ultrasound; intracellular delivery of macromolecules; Single-cell application; Optimized treatment conditions; epiblast stem cell

[*]Corresponding Author: Sangpil Yoon, Ph.D., 1042 Downey Way, DRB 128, Los Angeles, CA, 90089; sangpil@usc.edu; +1-213-821-2650.

Competing financial interests

The authors declare no competing financial interests.

Supplementary Information

Supplementary information was submitted with this manuscript.

Introduction

The intracellular delivery of cell membrane-impermeable molecules into the cytoplasm of cells has been one of the most attractive areas of research in biomedicine (Chen 2010; Glover et al. 2005; Kim et al. 2009; Leader et al. 2008; Shi et al. 2015). Controlling cellular functions and structures through delivering exogenous therapeutic or genetic materials into cells enables the exploration for visualization of specific cellular structures (Herce et al. 2013), analysis of cell mechanisms (Weill et al. 2008), and treatment of genetic diseases (Nabel et al. 1990). In these applications, investigations into unique expression profiles between individual cells at the single-cell level have had an increased emphasis on elucidation of potentially undetected particular cellular functions and structures of individual cells, and cell-to-cell interaction within a cell population (Chattopadhyay et al. 2014; Hoppe et al. 2014; Wang et al. 2009). A range of techniques such as virus-mediated transfection (Tanaka et al. 1997), lipid-mediated transfection (Felgner et al. 1987), microinjection (Meacham et al. 2014; Mehier-Humbert et al. 2005), electroporation (Escoffre et al. 2007; Mehier-Humbert et al. 2005; Palanker et al. 2006), and optical transfection (Mehier-Humbert et al. 2005; Watanabe et al. 2007; Zeira et al. 2006) to deliver foreign molecules into cells has been developed. Virus-mediated transfection is highly efficient, while viral vectors possess a limited packaging capacity and sometimes cannot be specifically integrated into the target cell. Lipid-mediated transfection has relatively low toxicity; however, transfection efficiency largely relies on cell types and culture conditions. Microinjection is straightforward and efficient, while this technique requires direct perforation of cell membranes, which may lead to physical damage to the cells. Electroporation and optical transfection have relatively high transfection efficiency; however, these methods may cause irreversible membrane damage under the influence of electrical fields and shorter wavelengths of laser radiation, respectively. Therefore, there is still a need for the development of approaches which are capable of simultaneously satisfying the requirements of high transfection efficiency, minimal cytotoxicity, and single-cell selectivity independent of cell types and transfer molecules (Antkowiak et al. 2013; Kawamura et al. 2009; Kim et al. 2010; Kollmannsperger et al. 2016; Nishikawa et al. 2008; Sharei et al. 2013).

Acoustic-transfection with high frequency ultrasound was developed in our laboratory as a new transfection method for delivering membrane-impermeable molecules into the cytoplasm of cells at ultrasound frequencies higher than 150 MHz (Yoon et al. 2015, 2016a, 2016b, 2017). A tightly focused high frequency ultrasound beam physically stretches cell lipid bilayer on plasma membranes, which generates transient and reversible holes on the cell membranes. The focused ultrasound beam was on only for a single ultrasound pulse of a few microseconds within an area of approximately 10 μm in diameter, which might result in the formation of a physical pathway for introducing membrane-impermeable molecules into cell cytoplasm and passive diffusion driven by the concentration gradient across transiently generated holes. We have also developed an impedance matching network to optimize excitation frequency of transducers (Kim et al. 2016). Acoustic-transfection technique was confirmed by the live-cell fluorescence imaging of the time-based intensity changes of delivered Ca^{2+} and propidium iodide (PI) molecule, and 3 kDa dextran labeled with Alexa

488 into HeLa cells at single-cell level. In addition, acoustic-transfection targets cells remotely with minimum cell toxicity (Yoon et al. 2016a, 2016b).

Additional experiments were necessary to determine the optimal acoustic-transfection conditions, which enable the acoustic-transfection technique to be a versatile and viable transfection tool. Optimal treatment conditions for the acoustic-transfection technique across different cell types and molecules were needed to achieve high delivery efficiency and high cell membrane permeability with minimizing membrane disruption.

In this paper, we give a detailed description of how optimal treatment conditions were determined to achieve high delivery efficiency with low cytotoxicity. Investigation into optimal treatment conditions of acoustic-transfection using high frequency ultrasound was performed on four human cancer cell lines; human cervical cancer cell (HeLa), Michigan cancer foundation-10A (MCF-10A), Michigan cancer foundation-7 (MCF-7), and M.D. Anderson-metastatic breast 231 (MDA-MB231). To find optimal treatment conditions, a criterion termed “intracellular delivery score (IDS)” was proposed and calculated from results—obtained on four human cancer cell lines—of (1) the delivery efficiency, (2) a cell membrane permeability study—which was measured by fluorescence intensity of propidium iodide (PI) after treatment on target cells—and (3) a cell viability study after 4 and 20 hours of treatment under different treatment conditions and a control condition. Adjustable parameters for acoustic-transfection were peak-to-peak voltage (V_{pp}), treatment time (T_t) and number of cycles and used at 6 different V_{pp} for 6 different T_t with 1 cycle. After performing live-cell fluorescence imaging of treated cells, the fluorescence intensity changes of PI inside treated cells under different treatment conditions were compared to those of background fluorescence intensity to quantify and calculate delivery efficiency and cell membrane permeability based on IDS. The cell viability study—the results of which were needed to compute IDS—was performed with a LIVE/DEAD Cell Imaging kit after 4 and 20 hours following the treatment. The IDS was plotted with respect to six values of V_{pp} at each of the six values of T_t in intracellular delivery graph (IDG) for easier viewing. We have chosen optimal treatment conditions if IDS is larger than 9 points in IDG, which indicates high delivery efficiency and high cell membrane permeability with minimum effects on cells. We conducted experiments on the intracellular delivery of 70 kDa dextran labeled with Oregon Green and simultaneous intracellular delivery of two molecules such as 70 kDa dextran and PI into the four human cancer cell lines using the optimal treatment conditions. By using one of the optimized treatment conditions, mCherry expressing DNA plasmid was delivered into epiblast stem cells to further confirm the performance of acoustic-transfection technique.

Materials and Methods

High frequency ultrasonic transducer and impedance matching network (IMN)

A single element lithium niobate ($LiNbO_3$) high frequency ultrasonic transducer was designed and fabricated with a previously reported approach (Lam et al. 2013). The aperture size and f_{number} of the fabricated ultrasonic transducer was 1 mm and 1, respectively. For the optimization of power transfer and efficiency by minimizing reflections between the ultrasonic transducer and the excitation source, custom-built impedance matching network

(IMN) was developed. After determining the suitable topology and component values of IMN using the Smith chart, IMN was optimized with a topology (series-added capacitor / shunt-added inductor) and component values (22 pF / 22 nH), and thus it was integrated with the ultrasonic transducer. A detailed description of the IMN optimization process for the high frequency ultrasonic transducers is demonstrated. (Kim et al. 2016). Figure 1a shows the pulse-echo waveform and echo spectrum obtained from the ultrasonic transducer with IMN and Figure 1b shows a B-mode wire target image along with the axial and lateral brightness profiles which were measured by scanning a 2.5 μm diameter tungsten wire target with a pulser/receiver generating energy of 1 μJ, receiver gain of 10 dB, pulse repetition frequency of 200 Hz, high pass filter of 30 MHz, and low pass filter of 300 MHz.. The measured center frequency, axial and lateral resolutions were 182 MHz, 21 μm and 9 μm, respectively.

Acoustic-transfection system with controllable treatment conditions

The acoustic-transfection system consists of fluorescence microscope and acoustic pulse generation system as shown in Figure 2. A fluorescence microscope (Leica DMI 4000B, Germany) was used to monitor fluorescence intensity changes of the treated cells, and was integrated with the tightly focused high frequency ultrasonic transducer with impedance matching network (IMN). A three dimensional linear translation/rotation stage controlled by a customized LabVIEW program was used to accurately place the location of the transducer during the experiments. The focus of the transducer was co-aligned with the focus of an objective lens of the microscope using a pulser/receiver and an oscilloscope. Acoustic pulses were generated by a function generator and a 50 dB power amplifier with controllable treatment conditions including peak-to-peak voltage (V_{pp}) and treatment time (T_t). The 6 different V_{pp} of 12V, 15V, 18V, 21V, 24V, and 27V with 6 different T_t of 6μs, 12μs, 18μs, 30μs, 60μs, and 90μs with 1 cycle were used.

Cell culture

HeLa, MCF-10A, MCF-7, MDA-MB231 cells were used in these studies. HeLa cells were cultured in eagle's minimum essential medium (EMEM) supplemented with 10% fetal bovine serum (FBS). MCF-7 and MDA-MB231 cells were cultured in dulbecco's modified eagle's medium (DMEM) supplemented with 10% FBS and 1% penicillin streptomycin. MCF-10A cells were cultured in mammary epithelial cell growth medium (MEGM Bullet Kit, Lonza, Basel, Switzerland) supplemented with 100 ng/ml cholera toxin (Sigma-Aldrich, St. Louis, MO). These cells were incubated in a humidified atmosphere of 5% CO_2 at 37°C and routinely sub-cultured in T25 vented-top culture flasks from two to three times per week. Cells were seeded in 35 mm grid petridishes (ibidi, Martinsried, Germany) with 2 mL of complete culture medium and incubated 36 hours in a humidified atmosphere.

Epiblast stem cells were cultured in Dulbecco's Modified Eagle Medium supplemented with 10% FBS, 1% MEM nonessential amino acids (Invitrogen), 0.1 mM β-mercaptoehanol (Invitrogen), 20 ng/mL of Activin A, 20 ng/mL of fibroblast growth factor, and 2.5 μM of IWR-1. Epiblast stem cells were incubated in 5% CO_2 at 37 C condition. For acoustic-transfection of mCherry plasmids, epiblast stem cells were seeded in 35 mm grid petridishes

24 hours before the experiments. The concentration of the mCherry plasmids were 100 ng/ul.

Live-cell fluorescence imaging and intracellular delivery score (IDS) for optimal treatment conditions

The effects of applied acoustic pulses on cells were recorded by using microscope imaging software (Leica LAS AF, Buffalo Grove, IL). We gently washed the cell monolayer on the prepared petridishes twice with 2 ml of phosphate-buffered saline (PBS), and added 50 μM of the propidium iodide (PI) solution to the cell monolayer. Live-cell fluorescence imaging was performed to quantify time-resolved PI fluorescence intensity and to compare the intensity between (1) before treatment which was related to PI(0) at 0 second and (2) after 3–5 minutes of treatment which was related to PI(∞) at steady-state. To extract quantitative information in a region of interest (ROI) in treated single cell, we performed imaging processing from live-cell fluorescence images by subtraction of a background region (ROB) next to ROI, which was previously described in references (McCloy et al. 2014; Ophir et al. 2013). Then, we averaged the effects of physical characteristics of cell size to directly check PI intensity comparison of individual cells among different human cancer cell lines even if the cells did not share similar physical characteristics including cell size. Consequently, the averaged PI intensity was calculated by using the following equation. The number of treated cells at each treatment condition was more than 5.

$$\mathrm{PI}_{\text{averaged intensity}}=\frac{[(ID\_ROI(\infty)-A\_ROI\cdot\overline{F}\_ROB(\infty))-(ID\_ROI(0)-A\_ROI\cdot\overline{F}\_ROB(0))]}{A\_ROI} \quad (1)$$

where Integrated density (ID) is the sum of the fluorescence intensity values of selected regions, area (A) is the selected regions in square pixels, mean fluorescence ($\bar{F}$) is the average fluorescence intensity value of selected regions, ID_ROI(∞) is the integrated density in ROI at steady-state, ID_ROI(0) is the integrated density in ROI at 0 second, A_ROI is the area in ROI, $\bar{F}$_ROB (∞) is the mean fluorescence in ROB at steady-state, and $\bar{F}$_ROB (0) is the mean fluorescence in ROB at 0 second.

For the cell viability study, the effects of treatment conditions and a control condition (0V / 0μs) on four human cancer cell lines were systemically investigated. After acoustic pulses were applied to the cells on the prepared petridishes, the monolayer was washed twice with 2 ml of PBS, and incubated with 2 ml fresh cell culture medium in a humidified atmosphere for 4 and 20 hours. Before acquiring live-cell fluorescence imaging, the cells were washed twice with 2 ml of PBS and stained with a LIVE/DEAD Cell Imaging kit (Life Technologies Corp., Carlsbad, CA) according to the manufacturer's instructions. Numbers of treated cells at each treatment condition were more than 6.

Table 1 gives the proposed criterion for intracellular delivery score (IDS) to find optimal treatment conditions using propidium iodide (PI). IDS considered delivery efficiency (D) and cell membrane permeability (P) in % out of 190 cells to assess the efficiency of acoustic-transfection technique for each cell line. Also, viability (V) after 4 and 20 hours of treatment in % out of 228 cells was used to estimate the safety of the acoustic-transfection technique. The percentage of delivery efficiency (D) was defined as the onset of small transient holes on cell membrane and calculated as the ratio of the number of delivered cells showing minimum propidium iodide (PI) intensity to the total number of the treated cells. The minimum PI intensity for calculating the percentage of delivery efficiency (D) was 0.01 arbitrary units (a.u.) of the averaged PI intensity because the value was a starting point, e.g. threshold of onset of small transient holes on cell membrane, to see delivery effects generated by high frequency ultrasound. Also, below 0.01 was very difficult to discern delivery effects because fluorescence level in region of interest (ROI) was very similar to fluorescence level in region of background (ROB) and there were no responses on treated cells at the time of treatment. The cell membrane permeability (P) was calculated and categorized according to the amount of the averaged PI intensity. The percentage of cell viability (V) was calculated as the ratio of the number of live cells to the total number of the treated cells. The final IDS was computed using a sum of the calculated values on the percentage of delivery efficiency (D), cell membrane permeability (P), and cell viability (V) according to the criterion defined for the IDS. We plotted IDS with respect to different V_{pp} at each of different T_t to clearly observe the effect on cells, which is intracellular delivery graph (IDG). The optimal treatment conditions were selected when IDS was above 9 on IDG.

Intracellular delivery of macromolecules and simultaneous intracellular delivery of two molecules using optimal treatment conditions

Now, we used optimal treatment conditions for the intracellular delivery of a 70 kDa dextran labeled with Oregon Green and simultaneous intracellular delivery of two molecules (70 kDa dextran and propidium iodide (PI)) into four kinds of human cancer cell lines. We added 35 μM of 70 kDa dextran solution for 70 kDa dextran intracellular delivery or 35 μM of 70 kDa dextran solution and 50 μM of the PI solution for simultaneous intracellular delivery to the cell monolayer. Before the treatment, bright-field images were acquired and then acoustic pulses were applied to the targeted cells. After the treatment, the monolayer was incubated in a humidified atmosphere for 30 minutes and washed twice with 2 ml of PBS. Then, bright-field and fluorescence images were taken to track and observe the presence of macromolecules in the treated cells. The percentage of 70 kDa dextran delivery efficiency was further calculated as the ratio of the number of delivered cells showing green fluorescence to the total number of the treated cells for each cell line under different optimal treatment conditions. Numbers of treated cells under each treatment condition were more than 5.

Results

Optimal treatment conditions on human cancer cell lines indicated by intracellular delivery score (IDS)

A detailed quantitative and mechanistic study was carried out to find optimal treatment conditions towards high delivery efficient with low cytotoxicity by controlling treatment conditions of acoustic-transfection given in the supplementary information (see Supplementary Figs. S1, S2, and S3 online). The intracellular delivery scores (IDS) for HeLa, MCF-7, MCF-10A and MDA-MB231 cells were calculated for varying treatment conditions. Figure 3 shows the intracellular delivery graph (IDG) after 4 and 20 hours of the treatment using the IDS on HeLa (Fig. 3a), MCF-7 (Fig. 3b), MCF-10A (Fig. 3c) and MDA-MB231 (Fig. 3d) cells for easier viewing.

Table 2 gives optimal treatment conditions which yields the IDS larger than 9 for the human cancer cell lines studied. According to IDS at 4 and 20 hours, optimal treatment conditions for each cell line were chosen as shown in table 2. These optimal treatment conditions were selected if cell viability was bigger than 90%.

Intracellular delivery of macromolecules with optimal treatment conditions

The intracellular delivery of 70 kDa dextran labeled with Oregon Green into HeLa, MCF-7, MCF-10A and MDA-MB231 cells under optimal treatment conditions is demonstrated in Figure 4 and the Supplementary information (see Supplementary Fig. S4 online). Left columns in Figure 4 indicate bright-field images before the treatment, and middle and right columns in Figure 4 show bright-field and fluorescence images after 0.5 hour of the treatment, respectively. Diffused green fluorescence was observed in the targeted cells while neighboring cells have no green fluorescence.

Optimal treatment conditions for simultaneous intracellular delivery of two molecules

Simultaneous intracellular delivery of 70 kDa dextran labeled with Oregon Green and propidium iodide (PI) into HeLa, MCF-7, MCF-10A and MDA-MB231 cells under optimal treatment conditions are shown in Figure 5 and the Supplementary information (see Supplementary Fig. S5 online). The first and second columns in Figure 5 indicate bright-field images before and after treatment, respectively, and the third and fourth columns in Figure 5 show fluorescence images of 70 kDa dextran labeled with Oregon Green and PI after 0.5 hour of the treatment, respectively, and the fifth columns in Figure 5 show overlapped images of the two different fluorescence images. It can be seen that delivered cells in the nucleus region emit red fluorescence due to the binding of PI molecules with nucleic acids, while the cytoplasmic staining of 70 kDa dextran labeled with Oregon Green is clearly observed.

Figure 6 illustrate intracellular delivery efficiency of 70 kDa dextran labeled with Oregon Green into HeLa, MCF-7, MCF-10A and MDA-MB231 cells under optimal treatment conditions, respectively. Therefore, the optimal treatment conditions for macromolecules (≤ 70 kDa) were those that achieved highest percentage of 70 kDa dextran delivery efficiency. Highest percentages of 70 kDa dextran delivery efficiency were 89% (16/18) with the

treatment condition of 24V / 30μs for HeLa cell, 83% (5/6) and 83% (15/18) with the treatment conditions are 24V / 30μs and 27V / 30μs, respectively for MCF-7 cell, 83% (5/6) with the treatment condition of 27V / 18μs for MCF-10A cell, 72% (13/18) with the treatment condition of 21V / 30μs for MDA-MB231 cell.

Large DNA plasmid delivery into epiblast stem cells

A DNA plasmid which expresses mCherry fluorescence was delivered into epiblast stem cells using acoustic-transfection. The size of the DNA was 8.9 kb. The delivery condition was 22V / 10 μs with 1 cycle. This condition was selected for safe delivery condition with high viability of epiblast stem cells. After 24 hours of treatment, treated cells were revisited and imaged with DIC and RFP channels. Daughter cells of originally treated cell were expressing mCherry signal as shown in Fig. 7. This result demonstrates that acoustic-transfection may be used to generate induced pluripotent stem cells by delivering one reprogramming factor into epiblast stem cell (Kim et al. 2013).

Discussion

In this paper, the exposure regime for optimized and safe intracellular delivery of macromolecules using acoustic-transfection with high frequency ultrasound is reported. Previously, acoustic-transfection with high frequency ultrasound successfully demonstrated the intracellular delivery of some small-sized molecules, which showed capabilities of low cytotoxicity and remote targeting at single-cell level. We have further conducted the investigation of treatment conditions to find optimized ultrasound exposure levels that allow efficient and safe delivery in this paper. Results on the intracellular delivery of a macromolecule such as 70 kDa dextran into four human cancer cell lines were acquired to determine whether acoustic-transfection is dependent on cell types and molecules to be delivered (Fan et al. 2013, Guzmán et al. 2001; Karshafian et al. 2009; Zeira et al. 2003). In order to shed light on these unresolved issues, the optimal treatment conditions of acoustic-transfection were determined, and utilized for the intracellular delivery of 70 kDa dextran labeled with Oregon Green and simultaneous intracellular delivery of two molecules namely, 70 kDa and propidium iodide (PI) to assess the acoustic-transfection as a method for efficient delivery of therapeutic or genetic materials. As described in Table 1 (see Materials and Methods for details), three parameters i.e., delivery efficiency, cell membrane permeability, and cell viability after 4 and 20 hours of the treatment were considered to determine the intracellular delivery score (IDS). The most crucial determinant factor among the three parameters is the cell viability. According to previously published studies, it has been reported that the highest percentage of 70 kDa dextran delivery efficiency was from 30% to 72% and at the same time, cell viability was less than 90% (Larina et al. 2005; Sharei et al. 2013; Song et al. 2015). In contrast, Figure 6 shows the highest percentage of 70 kDa dextran efficiency ranged from 72% to 89% and at the same time, cell viability was bigger than 90%. Therefore, the proposed criterion for the intracellular delivery score (IDS) enables the determination of optimal treatment conditions in various molecular size ranges from small-molecules to macromolecules by satisfying high delivery efficiency with minimal cell membrane disruption.

In this approach, our hypothesis was that it was possible to use a tightly focused high frequency ultrasound beam to disrupt the structural integrity of cell membranes and perhaps generate transient and reversible holes on cell membranes with merely the dose of a single ultrasound pulse of a few microsecond duration focused into an area of approximately 10 μm in diameter. The ultrasound energy may result in the formation of a physical pathway for introducing membrane-impermeable molecules into cell cytoplasm and passive diffusion driven by the concentration gradient across transiently generated holes. The hypothesis was further supported by intensive investigation of treatment conditions between different human cancer cell lines, intracellular delivery of a molecule from small-molecules to macromolecules, and simultaneous intracellular delivery of two molecules.

The dynamic behaviors of cell plasma membrane correlated with various treatment conditions were classified into four processes based on the intensive investigation of treatment conditions. First, the effects of the smallest V_{pp} and/or shortest T_t were observed for the lowest percentage of delivery efficiency, the lowest cell membrane permeability, and the highest percentage of cell viability, suggesting that the treatment conditions were not sufficient to induce significant disruption of cell membranes and deliver membrane-impermeable molecules into the cytoplasm of cells. Second, a slight increase in V_{pp} and/or T_t resulted in the disturbance of cell membranes and perhaps generation of small-scale transient holes on the cell membrane, diffusion-driven transport, and immediate sealing of the holes in the ruptured membrane, which allowed intracellular delivery of exogenous small-molecules (Yoon et al. 2016a) such as Ca^{2+} and propidium iodide (PI). Third, as V_{pp} and/or T_t were increased up to the threshold point of cell death from the second treatment conditions, increased disruption of cell membranes, passive diffusion across transiently generated holes, and sealing of the transient holes in the disturbed cell membrane were confirmed by intracellular delivery of small-molecules, macromolecules such as 3 kDa dextran and 70 kDa dextran, and even two molecules including PI and 70 kDa dextran. Fourth, the cell responses exposed to highest V_{pp} and/or longest T_t exhibited a remarkably high percentage of delivery efficiency, high cell membrane permeability; however, the lowest percentage of cell viability. It was postulated that these treatment conditions were sufficient to disrupt cell membranes and to prevent transient holes on the membrane from sealing themselves quickly, leading to permanent opening of the holes on the cell membrane and irreversible membrane damage. It can be estimated that 70 kDa dextran is bigger than the size of the nuclear envelope because fluorescent intensity from 70 kDa dextran labelled with Oregon green was much weaker in nuclear region as shown in in Figures 4 and 5, and Supplementary Figs. S4 and S5. Delivered cells in the nucleus region emitted red fluorescence with binding of PI to nucleic acids; on the other hand, the cells were mostly stained with 70 kDa dextran in cytoplasm region rather than nucleus region. A small amount of diffusion-driven 70 kDa dextran transport in the nucleus region was likely to have limited access to the nucleus region due to its molecular size compared with the nuclear membrane size. These results are in good agreement with previous published studies (Guzman et al. 2002; Larina et al. 2005).

Cell responses of different human cancer cell lines exposed to the treatment conditions were found to be different, suggesting that optimal treatment conditions may be cell dependent (Antkowiak et al. 2013; Larina et al. 2005; Mthunzi et al. 2010). For example, for the

delivery efficiency of 70 kDa dextran, the optimal treatment conditions were 24V / 30μs, which resulted in 89% delivery for HeLa cell and 83% for MCF-7 cell but only 57% for MCF-10A cell and 50% for MDA-MB231 cell. We highlighted some possibilities why different human cancer cell lines showed different responses to the same treatment condition based on the hypothesis of acoustic-transfection. Since our hypothesis was that the observed behavior was the result of the creation of a physical pathway in which transient and reversible holes were generated on the cell membranes, different cell responses might be attributed to considerably different physical and mechanical properties of human cancer cell lines including cell membrane recovery time related to elasticity of cell membranes and diameters of transiently generated holes on the surface of cell membranes determined by the membrane tensile strength. Therefore, to verify this hypothesis it will be necessary to extend our study to design and develop a system to allow simultaneous acoustic-transfection and membrane electrical impedance measurements to determine how the acoustic-transfection influences membrane dynamics of different cancer cell lines in the future.

There is a limitation of the present study. Measurement of acoustic pressure field for high frequency ultrasound in the frequency range higher than 60 MHz cannot be performed by using currently existing technology (Bleeker et al. 2000, Nagle et al. 2013, Umchid et al. 2009). As a result, treatment conditions represented by V_{pp} and T_t could not directly be converted to acoustic pressure, intensity, and energy, which has been a controversial issue. Therefore, the acoustic pressure generated by these tightly focused high frequency ultrasonic transducers was estimated with a commercial finite element modeling software (PZFlex, Cupertino, CA), and quantitatively simulated values of acoustic pressure filed at the focus of the transducer were plotted for treatment conditions of V_{pp} (12V, 15V, 18V, 21V, 24V, and 27V) and T_t (6μs, 12μs, 18μs, 30μs, 60μs, and 90μs) in the supplementary information (see Supplementary Fig. S6 online). It was found that the maximum pressures estimated under ideal conditions at the focal depth of the ultrasonic transducer were approximately 0.86 MPa (12V / 6μs – 90μs), 1 MPa (15V / 6μs – 90μs), 1.28 MPa (18V / 6μs – 90μs), 1.5 MPa (21V / 6μs – 90μs), 1.7 MPa (24V / 6μs – 90μs), and 2 MPa (27V / 6μs – 90μs), respectively. The mechanical index (MI) was further estimated as 0.15 which was calculated by dividing simulated values of maximum acoustic pressure field (2 MPa) by the square root of the center frequency (182 MHz) of the high frequency ultrasound beam. The MI of 0.15 was much lower than the maximum permitted value for the MI of 1.9 under the Food and Drug Administration (FDA) rules (FDA 1997). However, either the current device will have to be improved or new devices developed to allow experimental measurement of acoustic pressure, intensity, and energy for high frequency ultrasound in the range above 60 MHz. Moreover, we calculated the maximum temperature changes based on the mathematical modeling techniques (Nyborg. 1981, Cavicchi and O'Brien. 1984; Kim et al. 2017). We used FDA limitations (MI: 1.9, I_{sppa}: 190 W/cm^2) which may be much higher than our expected values for MI and I_{sppa}, and used maximum treatment time of 90μs. It is noted we used I_{sppa} instead of I_{spta} because intensity of a single ultrasound pulse of a few microseconds was considered to be the spatial peak value averaged over the duration of the pulse.

$$\Delta T_{max}=\frac{2\cdot\alpha\cdot I_{SPPA}\cdot\Delta t}{C_v}=0.06^{\circ}C \quad (2)$$

where α is 7.28 dB/cm at 182 MHz. I_{sppa} is 190 W/cm^2. Δt is 90μs. C_V is 4.18 J/cm^3 °C. From the estimated value of ΔT_{max} (0.06 °C), we concluded our approach has the potential of non-thermal effects with very minor thermal effects.

Controlling cell functions by efficiently and specifically introducing therapeutic or genetic materials into the targeted single cells with minimal effects on normal cell physiology is extremely useful for investigating induction of programmed cell death of cancer cells which is referred to as apoptosis and mapping of cellular signaling pathways (Elmore et al. 2007; Fesus et al. 1991; Matsushita et al. 2000). In these applications, the capability of single-cell targeting without significantly affecting surrounding cells is preferred. Since the signal pathways underlying apoptosis and intercellular interactions among a cell in apoptosis and its adjacent cells are still poorly understood, careful measurements of intracellular delivery of molecules including p53 tumor suppressor protein and Ca^{2+} may shed more light on extracellular and intracellular cell signaling pathways. Once the extracellular and intracellular signal pathways are precisely known, appropriate strategies on apoptosis-targeted therapies may be formulated and subsequently translated to clinical medicine for the treatment of numerous human diseases such as cancer.

Conclusions

A quantitative and mechanistic study of efficient and safe strategies for the optimized intracellular delivery of macromolecules across cell membranes using the acoustic-transfection with high frequency ultrasound was carried out. This approach entails the quantification of cell responses under varying treatment conditions for four human cancer cell lines, as measured by the intracellular delivery score (IDS) formulated based on the delivery efficiency, cell membrane permeability, and viability after 4 and 20 hours of the treatment. The optimal treatment conditions for the acoustic-transfection for the intracellular delivery of 70 kDa dextran labeled with Oregon Green and simultaneous intracellular delivery of two molecules, 70 kDa dextran and propidium iodide (PI), into these human cancer cell lines were determined. mCherry expressing DNA plasmid was delivered into epiblast stem cells by an optimized treatment condition of acoustic-transfection. The experimental results show that this approach is a viable tool for transporting molecules and particles across cell membranes in a safe and efficient manner.

Supplementary Material

Refer to Web version on PubMed Central for supplementary material.

Acknowledgments

This work was supported by the National Institutes of Health under grant No. P41-EB002182 to K. Kirk Shung. This work was also supported in part by NIH grant No. K99-GM120493-01A1 to Sangpil Yoon.

References

Antkowiak M, Torres-Mapa ML, Stevenson DJ, Dholakia K, Gunn-Moore FJ. Femtosecond optical transfection of individual mammalian cells. Nat Protoc. 2013; 8:1216–1233. [PubMed: 23722260]

Bleeker HJ, Lewin PA. A novel method for determining calibration and behavior of pvdf ultrasonic hydrophone probes in the frequency range up to 100 MHz. IEEE Trans Ultrason Ferroelectr Freq Control. 2000; 47:1354–1362. [PubMed: 18238681]

Chattopadhyay PK, Gierahn TM, Roederer M, Love JC. Single-cell technologies for monitoring immune systems. Nat Immunol. 2014; 15:128–135. [PubMed: 24448570]

Chen Z. Small-molecule delivery by nanoparticles for anticancer therapy. Trends Mol Med. 2010; 16:594–602. [PubMed: 20846905]

Elmore S. Apoptosis: a review of programmed cell death. Toxicol Pathol. 2007; 35:495–516. [PubMed: 17562483]

Escoffre JM, Hubert M, Dean DS, Rols MP, Favard C. Membrane perturbation by an external electric field: a mechanism to permit molecular uptake. Eur Biophys J. 2007; 36:973–983. [PubMed: 17576550]

Fan Z, Liu H, Mayer M, Deng CX. Improving ultrasound gene transfection efficiency by controlling ultrasound excitation of microbubbles. J Control Release. 2013; 170:401–413. [PubMed: 23770009]

FDA (US Food and Drug Administration). Information for manufacturers seeking marketing clearance of diagnostic ultrasound systems and transducers. Rockville, MD: Center for Devices and Radiological Health, US FDA; Sep 30. 1997

Felgner PL, Gadek TR, Holm M, Roman R, Chan HW, Wenz M, Northrop JP, Ringold GM, Danielsen M. Lipofection: a highly efficient, lipid-mediated DNA-transfection procedure. Proc Natl Acad Sci USA. 1987; 84:7413–7417. [PubMed: 2823261]

Fesus L, Davies PJ, Piacentini M. Apoptosis: molecular mechanisms in programmed cell death. Eur J Cell Biol. 1991; 56:170–177. [PubMed: 1802705]

Glover DJ, Lipps HJ, Jans DA. Towards safe, non-viral therapeutic gene expression in humans. Nat Rev Genet. 2005; 6:299–310. [PubMed: 15761468]

Guzmán HR, Nguyen DX, Khan S, Prausnitz MR. Ultrasound-mediated disruption of cell membranes. I. Quantification of molecular uptake and cell viability. J Acoust Soc Am. 2001; 110:588–596. [PubMed: 11508983]

Guzman HR, Nguyen DX, McNamara AJ, Prausnitz MR. Equilibrium loading of cells with macromolecules by ultrasound: effects of molecular size and acoustic energy. J Pharm Sci. 2002; 91:1693–1701. [PubMed: 12115831]

Herce HD, Deng W, Helma J, Leonhardt H, Cardoso MC. Visualization and targeted disruption of protein interactions in living cells. Nat Commun. 2013; 4:2660. [PubMed: 24154492]

Hoppe PS, Coutu DL, Schroeder T. Single-cell technologies sharpen up mammalian stem cell research. Nat Cell Biol. 2014; 16:919–927. [PubMed: 25271480]

Karshafian R, Bevan PD, Williams R, Samac S, Burns PN. Sonoporation by ultrasound-activated microbubble contrast agents: effect of acoustic exposure parameters on cell membrane permeability and cell viability. Ultrasound Med Biol. 2009; 35:847–860. [PubMed: 19110370]

Kawamura T, Suzuki J, Wang YV, Menendex S, Morera LB, Raya A, Wahl GM, Belmonte JCI. Linking the p53 tumour suppressor pathway to somatic cell reprogramming. Nature. 2009; 460:1140–1144. [PubMed: 19668186]

Kim D, Kim CH, Moon JI, Chung YG, Chang MY, Han BS, Ko S, Yang E, Cha KY, Lanza R, Kim KS. Generation of human induced pluripotent stem cells by direct delivery of reprogramming proteins. Cell Stem Cell. 2009; 4:472–476. [PubMed: 19481515]

Kim H, Wu J, Ye S, Tai C, Zhou X, Yan H, Li P, Pera M, Ying Q-L. Modulation of beta-catenin function maintains mouse epiblast stem cell and human embryonic stem cell self-renewal, Nat. Commun. 2013; 4:2403.

Kim MG, Yoon S, Kim HH, Shung KK. Impedance matching network for high frequency ultrasonic transducer for cellular applications. Ultrasonics. 2016; 65:258–267. [PubMed: 26442434]

Kim MG, Park J, Lim HG, Yoon S, Lee C, Chang JH, Shung KK. Label-free analysis of the characteristics of a single cell trapped by acoustic tweezers. Sci Rep. 2017; 7:14092. [PubMed: 29074938]

Kim TK, Eberwine JH. Mammalian cell transfection: the present and the future. Anal Bioanal Chem. 2010; 397:3173–3178. [PubMed: 20549496]

Kollmannsperger A, Sharei A, Raulf A, Heilemann M, Langer R, Jensen KF, Wieneke R, Tampé R. Live-cell protein labelling with nanometre precision by cell squeezing. Nat Commun. 2016; 7:10372. [PubMed: 26822409]

Lam KH, Hsu HS, Li Y, Lee C, Lin A, Zhou Q, Kim ES, Shung KK. Ultrahigh frequency lensless ultrasonic transducers for acoustic tweezers application. Biotechnol Bioeng. 2013; 110:881–886. [PubMed: 23042219]

Larina IV, Evers BM, Esenaliev RO. Optimal drug and gene delivery in cancer cells by ultrasound-induced cavitation. Anticancer Res. 2005; 25:149–156. [PubMed: 15816532]

Leader B, Baca QJ, Golan DE. Protein therapeutics: A summary and pharmacological classification. Nat Rev Drug Discov. 2008; 7:21–39. [PubMed: 18097458]

Matsushita H, Morishita R, Aoki M, Tomita N, Taniyama Y, Nakagami H, Shimozato T, Higaki J, Kaneda Y, Ogihara T. Transfection of antisense p53 tumor suppressor gene oligodeoxynucleotides into rat carotid artery results in abnormal growth of vascular smooth muscle cells. Circulation. 2000; 101:1447–1452. [PubMed: 10736291]

McCloy RA, Rogers S, Caldon CE, Lorca T, Castro A, Burgess A. Partial inhibition of Cdk1 in G 2 phase overrides the SAC and decouples mitotic events. Cell Cycle. 2014; 13:1400–1412. [PubMed: 24626186]

Meacham JM, Durvasula K, Degertekin FL, Fedorov AG. Physical methods for intracellular delivery: practical aspects from laboratory use to industrial-scale processing. J Lab Autom. 2014; 19:1–18. [PubMed: 23813915]

Mehier-Humbert S, Guy RH. Physical methods for gene transfer: improving the kinetics of gene delivery into cells. Adv Drug Deliv Rev. 2005; 57:733–753. [PubMed: 15757758]

Mthunzi P, Dholakia K, Gunn-Moore F. Phototransfection of mammalian cells using femtosecond laser pulses: optimization and applicability to stem cell differentiation. J Biomed Opt. 2010; 15:041507. [PubMed: 20799785]

Nabel EG, Plautz G, Nabel GJ. Site-specific gene expression in vivo by direct gene transfer into the arterial wall. Science. 1990; 249:1285–1288. [PubMed: 2119055]

Nagle SM, Moore MK, Sundar G, Schafer ME, Harris GR, Vaezy S, Gessert JM, Howard SM, Eaton RM. Challenges and regulatory considerations in the acoustic measurement of high-frequency (>20 MHz) ultrasound. J Ultrasound Med. 2013; 32:1897–1911. [PubMed: 24154893]

Nishikawa S, Goldstein RA, Nierras CR. The promise of human induced pluripotent stem cells for research and therapy. Nat Rev Mol Cell Biol. 2008; 9:725–729. [PubMed: 18698329]

Nyborg WL. Heat generation by ultrasound in a relaxing medium. J Acoust Soc Am. 1981; 70:310–312.

O'Brien WD Jr. Ultrasound-biophysics mechanisms. Prog Biophys Mol Biol. 2007; 93:212–255. [PubMed: 16934858]

Ophir MJ, Liu BC, Bunnell SC. The N terminus of SKAP55 enables T cell adhesion to TCR and integrin ligands via distinct mechanisms. J Cell Biol. 2013; 203:1021–1041. [PubMed: 24368808]

Palanker D, Chalberg T, Vankov A, Huie P, Molnar F, Butterwick A, Calos M, Marmor M, Blumenkranz MS. Plasma-mediated transfection of RPE. Proceedings SPIE Ophthalmic Technologies XVI. 2006; 6138:1–9.

Sharei A, Zoldan J, Adamo A, Sim WY, Cho N, Jackson E, Mao S, Schneider S, Han M, Lytton-Jean A, Basto PA, Jhunjhunwala S, Lee J, Heller DA, Kang JW, Hartoularos GC, Kim K, Anderson DG, Langer R, Jensen KF. A vector-free microfluidic platform for intracellular delivery. Proc Natl Acad Sci USA. 2013; 110:2082–2087. [PubMed: 23341631]

Shi C, Guo D, Xiao K, Wang X, Wang L, Luo J. A drug-specific nanocarrier design for efficient anticancer therapy. Nat Commun. 2015; 6:7449. [PubMed: 26158623]

Song KH, Fan AC, Brlansky JT, Trudeau T, Gutierrez-Hartmann A, Calvisi ML, Borden MA. High efficiency molecular delivery with sequential low-energy sonoporation bursts. Theranostics. 2015; 5:1419–1427. [PubMed: 26681986]

Tanaka T, Manome Y, Wen P, Kufe DW, Fine HA. Viral vector-mediated transduction of a modified platelet factor 4 cDNA inhibits angiogenesis and tumor growth. Nat Med. 1997; 3:437–442. [PubMed: 9095178]

Umchid S, Gopinath R, Srinivasan K, Lewin PA, Daryoush AS, Bansal L, EL-Sherif M. Development of calibration techniques for ultrasonic hydrophone probes in the frequency range from 1 to 100 MHz. Ultrasonics. 2009; 49:306–311. [PubMed: 19110289]

Wang M, Orwar O, Weber SG. Single-cell transfection by electroporation using an electrolyte/plasmid-filled capillary. Anal Chem. 2009; 81:4060–4067. [PubMed: 19351139]

Watanabe W, Arakawa N, Matsunaga S, Higashi T, Fukui K, Isobe K, Itoh K. Femtosecond laser disruption of subcellular organelles in a living cell. Opt Express. 2004; 12:4203–4213. [PubMed: 19483965]

Weill CO, Biri S, Adib A, Erbacher P. A practical approach for intracellular protein delivery. Cytotechnology. 2008; 56:41–48. [PubMed: 19002840]

Yoon S, Kim MG, Wang Y, Shung KK. Programmable delivery of macromolecules using high frequency ultrasound. Ultrasonics Symposium (IUS), 2015 IEEE International. 2015:1–3.

Yoon S, Kim MG, Chiu CT, Hwang JY, Kim HH, Wang Y, Shung KK. Direct and sustained intracellular delivery of exogenous molecules using acoustic-transfection with high frequency ultrasound. Sci Rep. 2016; 6:20477. [PubMed: 26843283]

Yoon S, Wang Y, Shung KK. Optimization of input parameters of acoustic-transfection for the intracellular delivery of macromolecules using FRET-based biosensors. Proc SPIE. 2016:9723.

Yoon S, Wang P, Peng Q, Wang Y, Shung KK. Acoustic-transfection for genomic manipulation of single-cells using high frequency ultrasound. Scientific Reports. 2017; 7:5275. [PubMed: 28706248]

Zeira E, Manevitch A, Khatchatouriants A, Pappo O, Hyam E, Darash-Yahana M, Tavor E, Honigman A, Lewis A, Galun E. Femtosecond infrared laser-an efficient and safe in vivo gene delivery system for prolonged expression. Mol Ther. 2003; 8:342–350. [PubMed: 12907157]

Zeira E, Manevitch A, Manevitch Z, Kedar E, Gropp M, Daudi N, Barsuk R, Harati M, Yotvat H, Troilo PJ 2nd, Griffiths TG, Pacchione SJ, Roden DF, Niu Z, Nussbaum O, Zamir G, Papo O, Hemo I, Lewis A, Galun E. Femtosecond laser: a new intradermal DNA delivery method for efficient, long-term gene expression and genetic immunization. FASEB J. 2007; 21:3522–3533. [PubMed: 17575264]

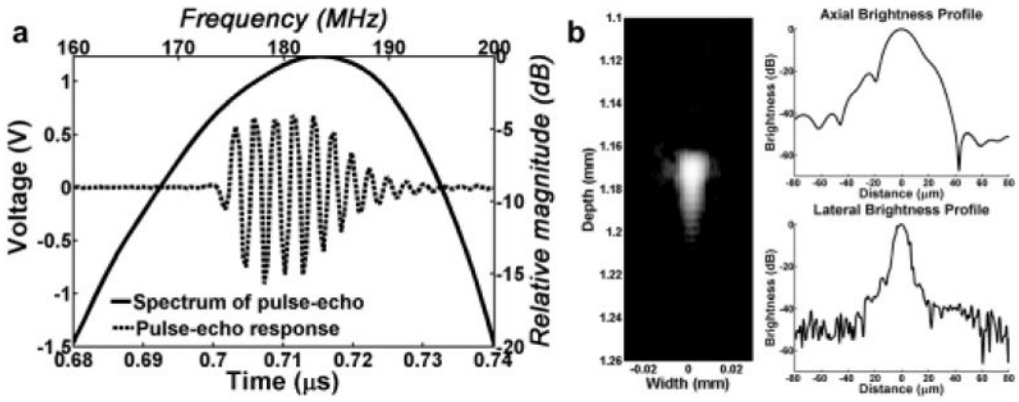

Fig. 1.

Measurement of developed ultrasonic transducer with impedance matching network (IMN). (a) Pulse-echo waveform and echo spectrum of the ultrasonic transducer with IMN. Measured center frequency was 182 MHz. (b) Measured B-mode image, axial and lateral resolutions of the ultrasonic transducer with IMN. The axial and lateral resolutions were 21 μm and 9 μm, respectively.

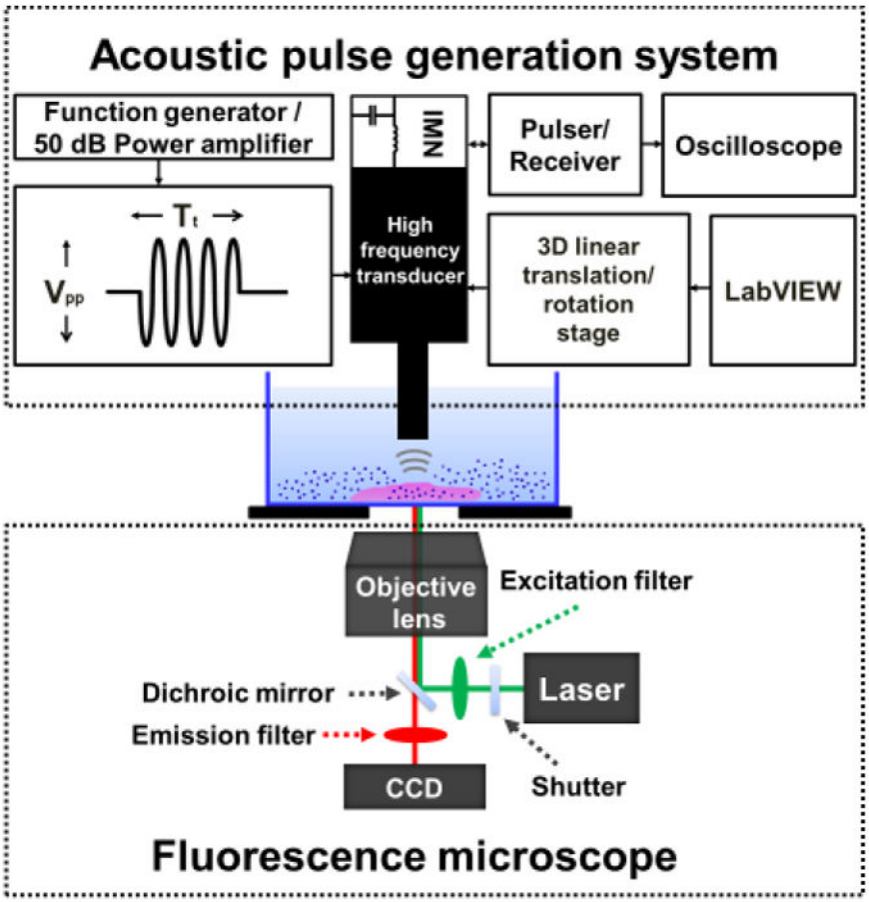

Fig. 2.

Acoustic-transfection system for intracellular delivery of membrane-impermeable molecules into cells. Fluorescence microscope was used to monitor live-cell fluorescence imaging on the targeted cells, and acoustic pulse generation system was utilized to precisely focus ultrasonic transducer with impedance matching network (IMN) and generate acoustic pulses with controllable treatment conditions such as peak-to-peak voltage (V_{pp}), treatment time (T_t).

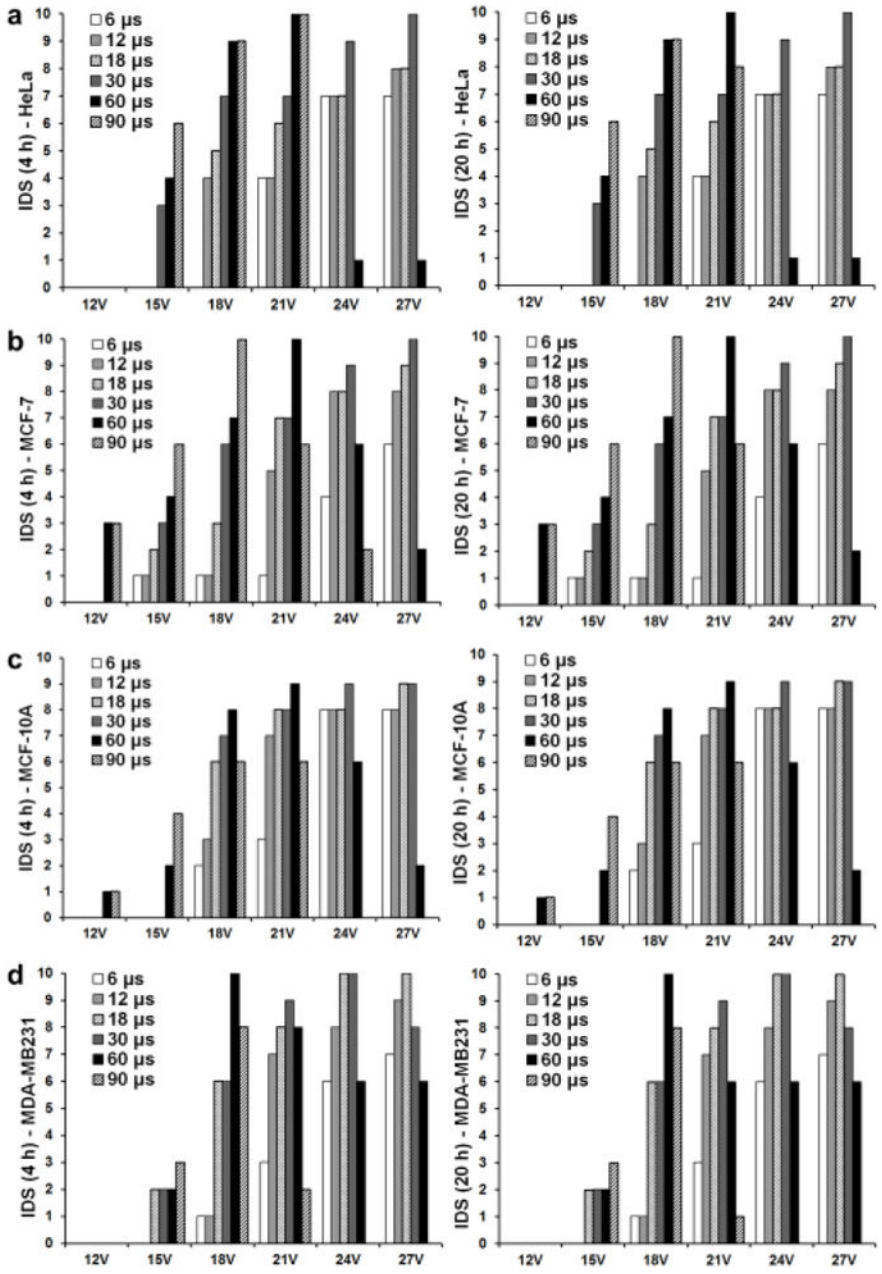

Fig. 3.

Intracellular delivery graph (IDG) using the intracellular delivery scores (IDS) after 4 and 20 hours of treatment for different treatment conditions. IDS is plotted on y-axis under six different V_{pp}. Six different T_t were applied at each V_{pp}. IDG after 4 and 20 hours was used to find optimal treatment conditions for (a) HeLa, (b) MCF-7, (c) MCF-10A, and (d) MDA-MB231 cell lines.

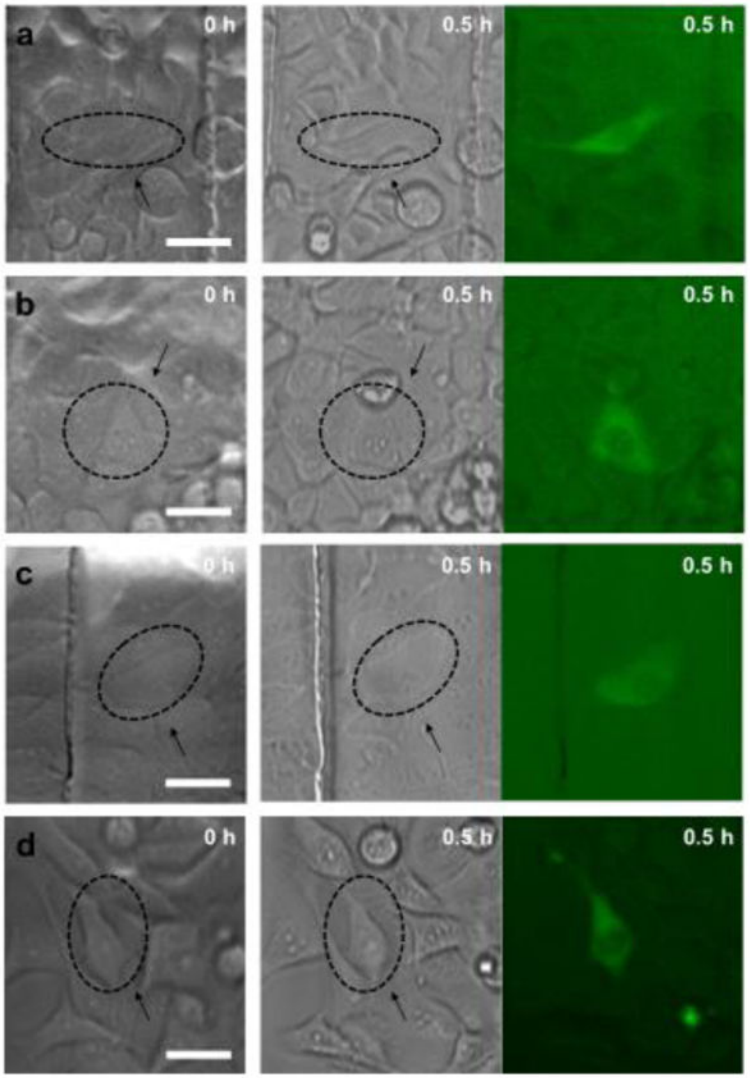

Fig. 4.

Intracellular delivery of 70 kDa dextran labeled with Oregon Green using optimal treatment conditions. Left column indicates bright-field images before the treatment, and middle and right columns show bright-field and fluorescence images after 0.5 hour of the treatment for (a) HeLa, (b) MCF-7, (c) MCF-10A, and (d) MDA-MB231 cell lines. Arrows show treated cells and scale bars indicate 40 μm.

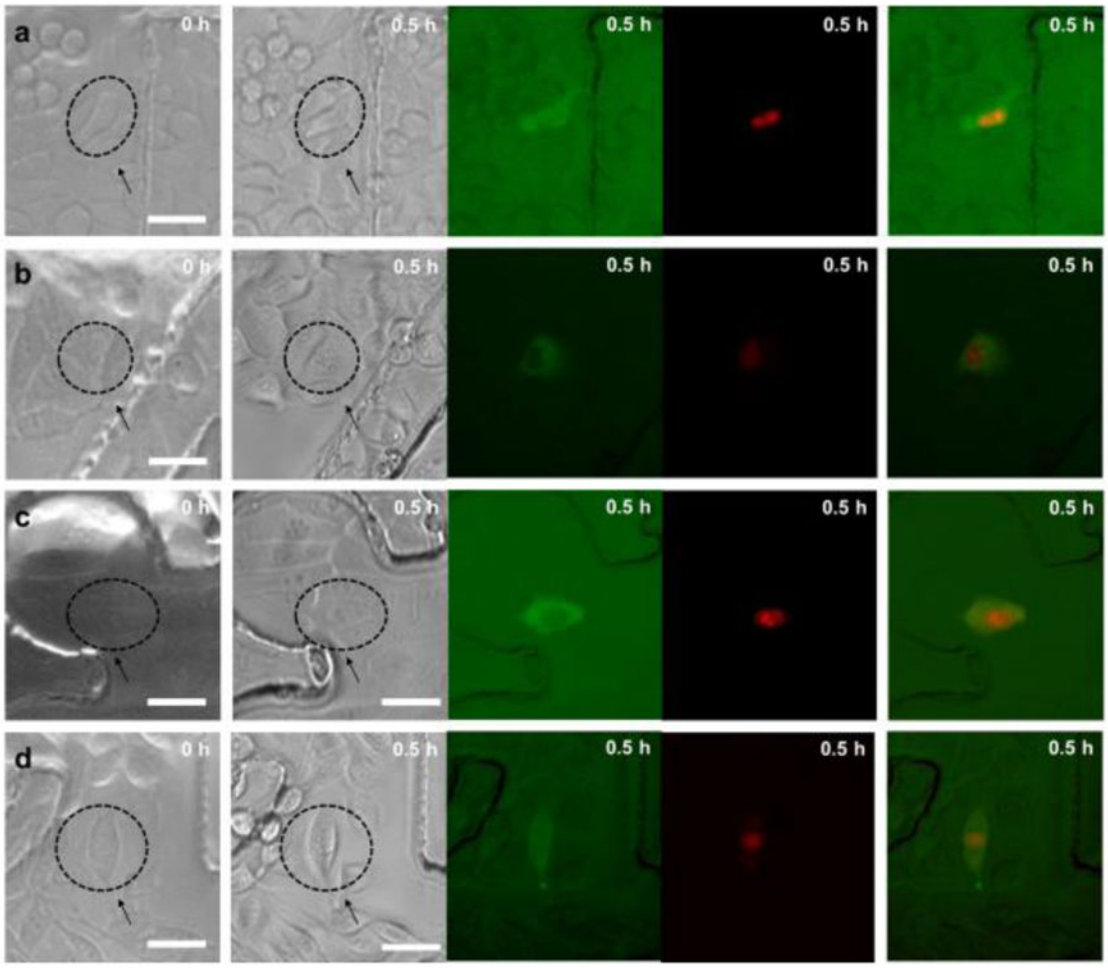

Fig. 5.

Simultaneous intracellular delivery of 70 kDa dextran labeled with Oregon Green and propidium iodide (PI) under optimal treatment conditions. The first and second columns indicate bright-field images before and after treatment, respectively, and the third and fourth columns show fluorescence images of 70 kDa dextran and PI after 0.5 hour of the treatment, respectively, and the fifth columns overlapped images of the two different fluorescence images for (a) HeLa, (b) MCF-7, (c) MCF-10A, and (d) MDA-MB231 cell lines. Arrows indicate treated cells and scale bars indicate 40 μm.

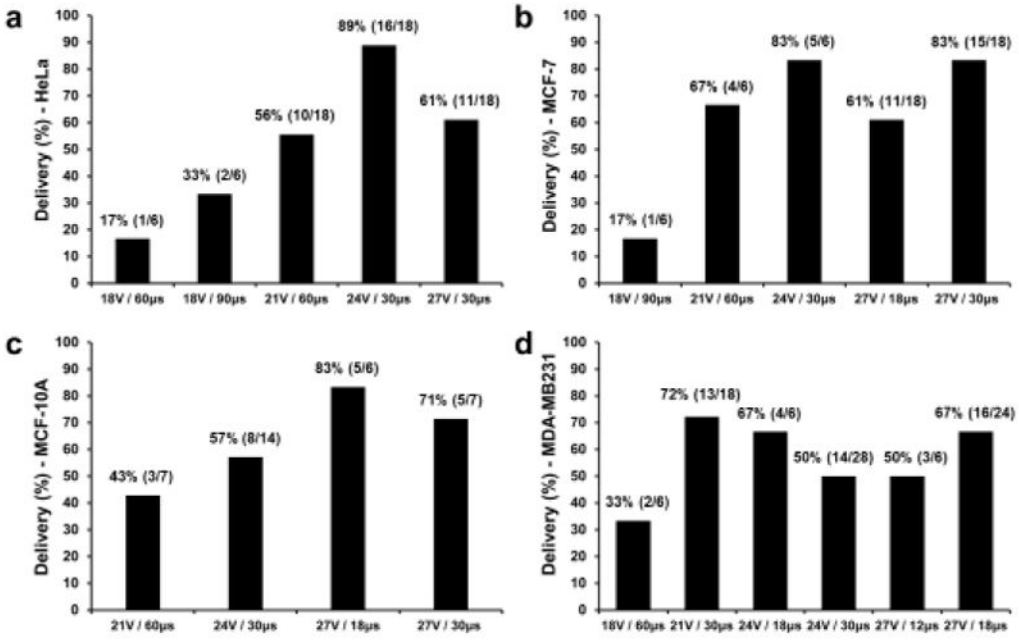

Fig. 6.

The intracellular delivery efficiency graph of macromolecules (70 kDa dextran labeled with Oregon Green) under optimal treatment conditions. (a) Highest percentage of 70 kDa dextran delivery efficiency is 89% (16/18) with the treatment condition of 24V / 30μs for HeLa cell. (b) Highest percentage of 70 kDa dextran delivery efficiency of 83% (5/6) and 83% (15/18) under treatment conditions are 24V / 30μs and 27V / 30μs, respectively for MCF-7 cell. (c) Highest percentage of 70 kDa dextran delivery efficiency is 83% (5/6) under the treatment condition of 27V / 18μs for MCF-10A cell. (d) Highest percentage of 70 kDa dextran delivery efficiency of 72% (13/18) under the treatment condition of 21V / 30μs for MDA-MB231 cell.

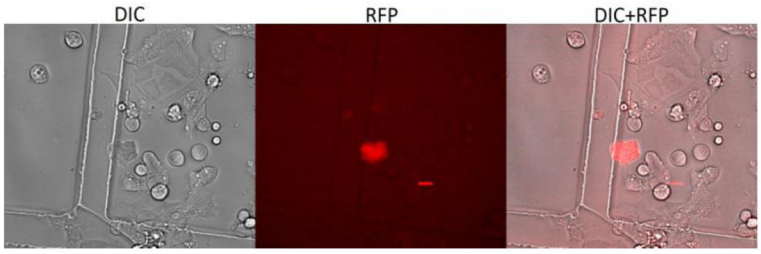

Fig. 7.

The intracellular delivery of mCherry plasmid into epiblast stem cells using acoustic-transfection. (a) DIC, (b) RFP, and (c) combined images of epiblast stem cells indicate that mCherry plasmids (8.9 kb) was successfully delivered into the target cell by acoustic-transfection. A scale bar indicates 20 μm.

Table 1

Criterion for the intracellular delivery score (IDS) to find optimal treatment conditions.

Criterion for the intracellular delivery score (IDS) which was categorized, and calculated by the interaction of the delivery efficiency (D), cell membrane permeability (P), and cell viability (V) after 4 and 20 hours of treatment.

Delivery efficiency		Permeability		Viability	
90% ≤ D	+5	15 ≤ P	+5	90% ≤ V	−0
70% ≤ D < 90%	+4	10 ≤ P < 15	+4	70% ≤ V < 90%	−2
50% ≤ D < 70%	+3	5 ≤ P < 10	+3	50% ≤ V < 70%	−4
30% ≤ D < 50%	+2	1 ≤ P < 5	+2	30% ≤ V < 50%	−8
10% ≤ D < 30%	+1	0.01 ≤ P < 1	+1	10% ≤ V < 30%	−9
D < 10%	+0	P < 0.01	+0	V < 10%	−10

Table 2

Intracellular delivery score (IDS) larger than 9 were defined as optimal treatment conditions using propidium iodide (PI) for the delivery efficiency (D) and cell membrane permeability (P) and LIVE/DEAD Cell Imaging kit for cell viability (V).

Intracellular delivery score (IDS) were defined as optimal treatment conditions for small-molecules, which enabled simultaneous satisfaction of high percentage of delivery efficiency and high cell membrane permeability with minimal influence to cells.

HeLa				MCF-7				MCF-10A				MDA-MB231			
V_{pp} (V)	T_t (μs)	IDS		V_{pp} (V)	T_t (μs)	IDS		V_{pp} (V)	T_t (μs)	IDS		V_{pp} (V)	T_t (μs)	IDS	
		4 hr	20 hr			4 hr	20 hr			4 hr	20 hr			4 hr	20 hr
18	60	9	9	18	90	10	10	21	60	9	9	18	60	10	10
18	90	9	9	21	60	10	10	24	30	9	9	21	30	9	9
21	60	10	10	24	30	9	9	27	18	9	9	24	18	10	10
24	30	9	9	27	18	9	9	27	30	9	9	24	30	10	10
27	30	10	10	27	30	10	10	-	-	-	-	27	12	9	9
-	-	-	-	-	-	-	-	-	-	-	-	27	18	10	10